

A second glance at SN 2002ap and the M 74 field with *XMM-Newton*

Roberto Soria¹, Elena Pian² and Paolo A. Mazzali²

¹ Mullard Space Science Laboratory, University College London, Holmbury St Mary, Surrey RH5 6NT, UK
email: Roberto.Soria@mssl.ucl.ac.uk

² INAF, Osservatorio Astronomico di Trieste, via Tiepolo 11, I-34131 Trieste, Italy
email: pian@ts.astro.it, mazzali@ts.astro.it

Received 29 April 2003; Revised 04 September 2003

Abstract. We have re-observed the field of M 74 in January 2003 with *XMM-Newton*, 11 months after the X-ray detection of SN 2002ap. From a comparison of the two *XMM-Newton* observations we obtain more accurate values for the X-ray luminosity and colours of the source five days after the event, and a limit on its decline rate. We compare its X-ray behaviour (prompt soft X-ray emission, relatively low luminosity) with that of other Type Ic SNe, and speculate that SN 2002ap may share some physical properties (low mass-loss rate and high-velocity stellar wind from the progenitor star) with the candidate hypernova/gamma-ray-burst progenitor SN 1998bw, but with a lower (non-relativistic) speed of the ejecta. We suggest that the X-ray emission observed in 2002 is likely to come from the radiatively-cooling reverse shock, at a temperature $kT \approx 0.8$ keV, and that this soft component was already detected 5 d after the event because the absorbing column density of the cool shell between the forward and reverse shocks was only $\sim 10^{20} \text{ cm}^{-2}$, ie, the shell was optically thin in the soft X-ray band. The new *XMM-Newton* data also allowed us to continue monitoring two bright variable sources in M 74 that had reached peak luminosities $> 10^{39} \text{ erg s}^{-1}$ in previous *XMM-Newton* and *Chandra* observations. Finally, we used two *Chandra* observations from 2001 to investigate the luminosity and colour distribution of the X-ray source population of M 74, typical of moderately-active late-type spirals.

Key words. Galaxies: individual (M 74) – Galaxies: spiral – Supernovae: individual (SN 2002ap) – X-rays: binaries – X-rays: galaxies

1. Introduction

To date, only about 20 supernovae (SNe) have been detected in the X-ray band (see Schlegel 1995; Immler et al. 1998; Schlegel 1999; Pian et al. 2000; Immler et al. 2001; Pooley et al. 2002; Schlegel 2001; Immler et al. 2002; and the recent review by Immler & Lewin 2002). Most studies have been conducted in the soft X-ray band by *ROSAT* and more recently by *Chandra* and *XMM-Newton* (Fox et al. 2000; Kulkarni & Fox 2003; Pooley & Lewin 2002; Schlegel 2002; Zimmermann & Aschenbach 2003). Information at harder energies is much more limited: only SNe 1987A, 1993J and 1998bw have been investigated at energies higher than 13 keV, and only the first two have been detected (Sunyaev et al. 1987; Inoue et al. 1991; Leising et al. 1994).

SN 2002ap in M 74 (NGC 628) is one of only four Type Ic SNe detected in the X-rays, the others being the low-mass, normally energetic SN 1994I (Immler et al. 1998; Immler et al. 2002), the massive and energetic “hypernova” SN 1998bw (Galama et al. 1998; Iwamoto et al. 1998; Pian et al. 2000), and the normal SN 2003L (Boles et al. 2003; Kulkarni & Fox 2003; Matheson et al. 2003). From its broad optical spectral features

and its high kinetic energy, Mazzali et al. (2002) argued that SN 2002ap can be classified as a hypernova, a class of SNe characterised by an energetic, probably asymmetric explosion and by a large mass of the collapsing star (Paczynski 1998; MacFadyen & Woosley 1999). These physical circumstances make hypernovae strong candidates to explain the origin of gamma-ray bursts (GRBs). Indeed, SN 1998bw was observed in the *BeppoSAX* error box of GRB980425 and showed a good temporal agreement with it. Hypernovae are also thought to be progenitors of stellar-mass and possibly intermediate-mass black holes (BHs). Studying a Type Ic event at all wavelengths, and especially at high energies, is therefore crucial to understand the possible link between GRBs and SNe, and to test the identification of hypernovae as Type Ic SNe.

The host galaxy of SN 2002ap is itself an interesting target for an X-ray study: it is a face-on (inclination angle $< 7^\circ$, Shostak & van der Kruit 1984), late-type spiral (morphological type Sc), with star formation along well-defined arms (eg, Kennicutt & Hodge 1980). Its distance remains uncertain: recent photometric measurements put it at 7.3 Mpc (Sharina et al. 1996; Sohn & Davidge 1996). Previous estimates, however, ranged from 2 to 20 Mpc (eg, Bottinelli et al. 1984; Sandage & Tammann 1974). A distance of 8.8 Mpc was recently adopted

by Huchra et al. (1999) based on its redshift. In this paper we shall assume a distance of 7.3 Mpc for all flux-to-luminosity conversions.

2. Data analysis and Results

2.1. Log of the observations

The field of SN 2002ap and its host galaxy M 74 were observed by all instruments on board *XMM-Newton* with two Target-of-Opportunity observations: the first on 2002 February 2.03–2.42 UT (revolution 394, less than 5 days after the SN event); the second on 2003 January 7.53–7.83 UT (revolution 564). Both were taken in full frame, thin filter mode. After rejecting intervals characterised by highly fluctuating background, we kept a good time interval of 21.5 ks for the 2002 pn observation, and 20.9 ks for the 2003 one. For the MOS, the good-time intervals were 23.7 ks in 2002 and 24.4 ks in 2003. We processed both datasets, and extracted spectra and lightcurves using version 5.4 of the XMM-Science Analysis Software (SAS); we considered only “pattern-0” events in both pn and MOS. We then used standard tools such as XSPEC (Arnaud 1996) for further data analysis.

In addition to the 2002 and 2003 *XMM-Newton* observations, M 74 was observed twice by *Chandra* ACIS-S: on 2001 June 19 (46.4 ks), and on 2001 October 19 (46.2 ks). On both occasions, the back-illuminated S3 chip was used. We obtained the *Chandra* dataset from the public archive and analysed it with the standard CIAO software. We inspected the background count rates during the two exposures, and chose to retain both intervals in full (See also Krauss et al. (2003)). We used standard source-finding routines (*wavdetect* and *celldetect*, which give similar results) to identify the point sources. To increase the signal-to-noise ratio of faint sources, we also built a merged event file from the two *Chandra* observations, and used it to compile a source list and their average count rates in the full energy band (0.3–8 keV) and in three narrower bands (Table A.1).

2.2. Count rates for SN 2002ap

SN 2002ap is not detected in the 2003 January observation: neither in the single pn and MOS images, nor in a combined EPIC image. By comparison with the detection limit of the faintest sources in the combined image, we estimate a 3 sigma upper limit to the EPIC pn count rate of $\approx 4 \times 10^{-4}$ cts s⁻¹ in the 0.3–12 keV band.¹

Instead, SN 2002ap is detected as an X-ray source in the 2002 February observation, both in the EPIC pn and in the EPIC MOS images. A preliminary estimate (Sutaria et al. 2002) yielded an observed flux of $1.07^{+0.63}_{-0.31} \times 10^{-14}$ erg cm⁻² s⁻¹ in the 0.3–10.0 keV band. Sutaria et al. (2002) obtained this value by extracting the events from a 40'' circle centred on the optical position of SN 2002ap, then subtracting the contribution from the background and from an unrelated source

(CXOU J013623.5+154458) located $\approx 15''$ from the SN. The contribution from CXOU J013623.5+154458 was estimated from the archival *Chandra* ACIS observation of M 74 taken on 2001 October 19. However, this method may lead to an inaccurate estimate, given the large uncertainty in the spectrum of CXOU J013623.5+154458 (ACIS-S count rate of 5.7×10^{-4} cts s⁻¹, ie, only 26 counts in the 46.2-ks *Chandra* observation). Moreover, a 40'' extraction radius includes a significant contribution from at least one other *Chandra* source (CXOU J013626.6+154458), located 38'' from the SN (ACIS-S count rate of 1.9×10^{-4} cts s⁻¹).

We obtained an improved estimate of the X-ray flux of SN 2002ap in two different ways. Firstly, we used a much smaller extraction region (12'' radius), to reduce the contamination from CXOU J013623.5+154458 and CXOU J013626.6+154458. We used the latest SAS calibration files, to correct for the smaller energy fraction enclosed in this region ($\approx 60\%$ of the total, for channel energies $\lesssim 2$ keV). We used the SAS tasks *rmfgen* and *arfgen* to construct accurate response matrices at the position of the source. The background was extracted from the same pn chip, in a region that did not contain any detected sources.

Alternatively, we used the 2003 image as a background to be subtracted from the 2002 dataset. To make sure we could do that, we compared the background contribution in the good-time-intervals of the 2002 and 2003 EPIC datasets. The (low) background count rate in the 0.3–12 keV range is consistent with being the same in both observations (differences are $< 2\%$ for the pn, and $< 5\%$ for the MOS). The pointing of the spacecraft was also approximately the same in 2002 and 2003, hence SN 2002ap is located in the same chip, nearly on-axis on both occasions. Comparing the *XMM-Newton* and *Chandra* datasets, we could verify that the brighter (and closer) of the two *Chandra* sources, CXOU J013623.5+154458, does not show significant flux variations from 2001 to 2003. Therefore, we assumed that its state in 2002 was similar to that displayed in 2001 and 2003. If we assume that other possible faint sources in the region around SN 2002ap did not vary between 2002 and 2003, we can subtract the flux detected at the position of SN 2002ap in the 2003 observation from the value measured in 2002. This gives us at least a lower limit on the luminosity of SN 2002ap in 2002.

Applying the first method (ie, using the 2002 dataset only, for source and background), we obtain a pn count rate of $(2.75 \pm 0.57) \times 10^{-3}$ cts s⁻¹ in the 0.3–12 keV band. By comparing the count rates in three separate narrow bands (0.3–1 keV, 1–2 keV, 2–12 keV) we notice that the source has a soft spectrum. In fact, the count rate in the 2–12 keV band is affected by some residual contamination from the nearby hard spectrum source CXOU J013623.5+154458, and should be considered an upper limit to the hard X-ray emission from SN 2002ap. For MOS1, the corrected count rate on 2002 February 2 was $(7.0 \pm 2.7) \times 10^{-4}$ cts s⁻¹; for MOS2, $(7.8 \pm 2.9) \times 10^{-4}$ cts s⁻¹. The low number of source counts (≈ 10 counts in each of the two detectors) does not allow a significant colour determination from the MOS's.

We then applied the second method, analysing the difference in the emission at the position of SN 2002ap between 2002 and 2003. We used two different source extraction radii:

¹ All the count rates listed here and hereafter have already been corrected for the enclosed energy fraction and the vignetting.

for a $12''$ radius, we obtain that the pn count rate in 2002 was higher than in 2003 by $(2.6 \pm 0.5) \times 10^{-3}$ cts s^{-1} in the 0.3–12 keV band. When a $30''$ circle is used, the differential pn count rate is $(3.0 \pm 0.7) \times 10^{-3}$ cts s^{-1} in the same energy band. Applying the same method to the MOS1 dataset, we obtain a differential count rate of $(8.6 \pm 2.8) \times 10^{-4}$ cts s^{-1} in the 0.3–12 keV band when we use a $12''$ extraction region, and $(6.9 \pm 3.8) \times 10^{-4}$ cts s^{-1} for a $30''$ circle. For MOS2, the count rates are $(7.5 \pm 2.9) \times 10^{-4}$ cts s^{-1} and $(7.5 \pm 3.8) \times 10^{-4}$ cts s^{-1} , respectively. These values are consistent with the respective pn and MOS count rates determined from the 2002 dataset alone with the previous method, confirming that the contribution of SN 2002ap in 2003 is negligible.

Taking the average of the three measurements for each detector, we obtain the pn, MOS1 and MOS2 count rates listed in Table 1. In the same table we have also reported the count rates in separate energy bands. The errors quoted in Table 1 are the errors in the mean from the three measurements (Gaussian propagation).

We point out that the analysis presented in this section supersedes the preliminary report on the X-ray colors and luminosity of SN 2002ap published in Sect. 4.2 of Soria & Kong (2002). In that paper, we said that the source was very hard: in fact, this was caused by contamination from the nearby hard source CXOU J013623.5+154458, which has been properly subtracted here with the help of the Chandra datasets.

2.3. Flux and luminosity of SN 2002ap

The low signal-to-noise ratio of the pn spectrum does not allow a meaningful model fitting in XSPEC. However, we can at least constrain the spectrum of SN 2002ap by comparing its soft and hard X-ray colours with the colours expected for some simple spectral models. The count rates inferred for the three pn narrow bands on 2002 February 2 (Table 1) are indicative of a soft spectrum. The conversion from count rates to emitted fluxes is strongly dependent on the absorbing column density. The foreground Galactic HI column density in the direction of M 74 has been estimated as 4.8×10^{20} cm^{-2} (Dickey & Lockman 1990). From the interstellar dust maps of Schlegel et al. (1998), a reddening $E(B - V) = 0.072 \pm 0.012$ is obtained at the position of SN 2002ap. Using the empirical relation $n_H = 1.79 \times 10^{21} A_V = 5.73 \times 10^{21} E(B - V)$ cm^{-2} (Predehl & Schmitt 1995), where A_V is the extinction in the V band, a Galactic column density $n_H = 4.2^{+0.6}_{-0.7} \times 10^{20}$ cm^{-2} is derived. To this value, we need to add the intrinsic absorption due to the circumstellar material. For this component, optical spectroscopic analysis of the Na I D lines shows that $n_H = (1.15 \pm 0.05) \times 10^{20}$ cm^{-2} (Takada-Hidai et al. 2002). Hence, we can take 5×10^{20} cm^{-2} as a lower limit on the total absorbing column density. However, the X-ray spectrum may be more absorbed than the optical emission, hence we cannot obtain an upper limit for n_H from the optical observations. We shall discuss this issue in Section 3.1.

We then assumed that the spectrum could be approximated by one or two optically-thin thermal-plasma components (Raymond-Smith models in XSPEC, with solar abundance), and

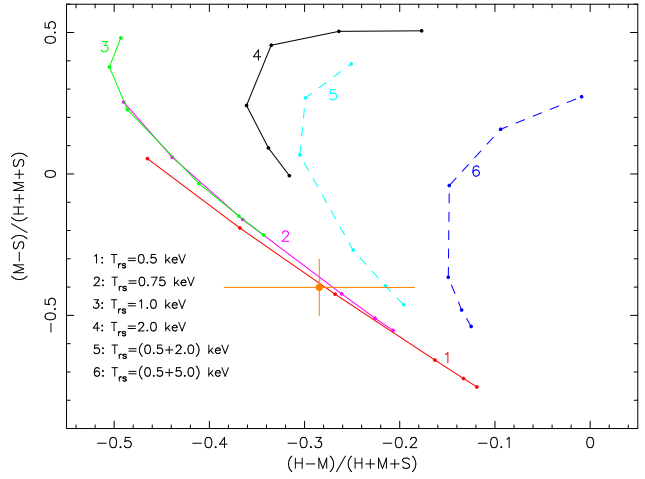


Fig. 1. Observed colours of SN 2002ap on 2002 February 2. Here S is the pn count rate in the 0.3–1 keV band, M is the rate in the 1–2 keV band, and H the rate in the 2–12 keV band (as listed in Table 1). The curves show the expected colours for some simple one- and two-temperature Raymond-Smith spectral models, at varying column densities. Along each curve, we plotted the colours corresponding to $n_H = (0.5, 1.0, 2.0, 5.0, 7.5, 10) \times 10^{21}$ cm^{-2} (column density increasing from the bottom to the top along each curve).

we investigated the range of temperatures and column densities consistent with the observed colours. We found (Fig. 1) that the spectrum is inconsistent with single-temperature models at $kT \gtrsim 1$ keV. The observed X-ray colours are consistent for example with a single-temperature model with $kT \approx 0.5$ keV and $n_H \approx 5 \times 10^{21}$ cm^{-2} ; or with $kT \approx 0.75$ keV and $n_H \approx 3 \times 10^{21}$ cm^{-2} . If we take the lowest allowed value of $n_H \approx 5 \times 10^{20}$ cm^{-2} , the observed colours imply $kT \approx 0.85$ keV. We cannot rule out two-temperature models, for example, with $kT_1 \approx 0.5$ keV, $kT_2 \approx 2$ keV, $n_H \approx 1 \times 10^{21}$ cm^{-2} , where we have normalized the two components so that each contributes half of the emitted flux in the 0.3–12 keV band. However, two-temperature models including a hot component with $kT \gtrsim 5$ keV are inconsistent with the soft colours observed for this source.

We calculated the fluxes for some representative single-temperature models consistent with the observed colours (Table 2). As noted earlier, most of the X-ray flux is detected below 2 keV. We estimate an emitted luminosity in the 0.3–2 keV band ranging from a few times 10^{37} to $\approx 10^{38}$ erg s^{-1} (depending on the spectral model), and an emitted luminosity in the 2–12 keV band of $\approx 1.2 \times 10^{36}$ erg s^{-1} for all spectral models. However, given the large uncertainties in the background subtraction, we can take $\approx 1 \times 10^{37}$ erg s^{-1} as a safe upper limit for the emitted luminosity in the hard band. A distance of 7.3 Mpc has been assumed.

2.4. Two “ultra-luminous” sources?

Two variable X-ray sources were detected by *XMM-Newton* with peak emitted luminosities $\gtrsim 10^{39}$ erg s^{-1} . One of them,

Table 1. *XMM-Newton* count rates for SN 2002ap on 2002 February 2, in units of 10^{-4} cts s^{-1} . The rates have been corrected for the telescope vignetting and the finite size of the extraction region. The values listed here are the averages of the results obtained with the three measurements described in Section 2.2.

Instrument	Count rate (0.3–12.0) keV	Count rate (0.3–1) keV	Count rate (1–2) keV	Count rate (2–12) keV
EPIC pn	27.8 ± 3.4	19.5 ± 2.6	8.2 ± 1.6	0.3 ± 2.0
EPIC MOS1	7.5 ± 1.8			
EPIC MOS2	7.6 ± 1.9			

Table 2. Observed and emitted fluxes of SN 2002ap on 2002 February 2, for three different spectral models consistent with the observed X-ray count rates in the EPIC pn and MOS bands (Table 1). A distance of 7.3 Mpc has been assumed. Fluxes are in units of 10^{-15} erg cm^{-2} s^{-1} .

Instrument	Flux (0.3–12.0) keV	Flux (0.3–1) keV	Flux (1–2) keV	Flux (2–12) keV
model: $n_H = 5 \times 10^{21} \text{ cm}^{-2}$; $kT_{\text{rs}} = 0.50 \text{ keV}$; $Z = Z_{\odot}$				
pn observed flux	4.9 ± 0.6	2.8 ± 0.4	1.9 ± 0.4	0.2 ± 1.2
MOS1 observed flux	4.0 ± 1.0			
MOS2 observed flux	4.1 ± 1.0			
pn emitted flux	25.7 ± 3.1	21.5 ± 2.9	3.9 ± 0.8	0.2 ± 1.2
MOS1 emitted flux	21.1 ± 5.1			
MOS2 emitted flux	21.4 ± 5.2			
model: $n_H = 3 \times 10^{21} \text{ cm}^{-2}$; $kT_{\text{rs}} = 0.75 \text{ keV}$; $Z = Z_{\odot}$				
pn observed flux	5.2 ± 0.6	2.9 ± 0.4	2.0 ± 0.4	0.2 ± 1.2
MOS1 observed flux	4.1 ± 1.1			
MOS2 observed flux	4.2 ± 1.1			
pn emitted flux	12.4 ± 1.5	9.2 ± 1.2	3.1 ± 0.7	0.2 ± 1.2
MOS1 emitted flux	9.9 ± 2.4			
MOS2 emitted flux	10.0 ± 2.4			
model: $n_H = 0.5 \times 10^{21} \text{ cm}^{-2}$; $kT_{\text{rs}} = 0.85 \text{ keV}$; $Z = Z_{\odot}$				
pn observed flux	5.0 ± 0.6	2.8 ± 0.4	2.0 ± 0.4	0.2 ± 1.2
MOS1 observed flux	4.1 ± 1.1			
MOS2 observed flux	4.2 ± 1.1			
pn emitted flux	5.9 ± 0.7	3.6 ± 0.5	2.0 ± 0.4	0.2 ± 1.2
MOS1 emitted flux	4.9 ± 1.3			
MOS2 emitted flux	5.0 ± 1.3			

XMMU J013636.5+155036, was detected only in the 2002 February EPIC observation (Soria & Kong 2002). It was not found in the 2003 January co-added EPIC image, from which we estimate that it was at least 30 times fainter than 11 months before, in the 0.3–12 keV band. It was also undetected in both *Chandra* images from 2001. We refined the spectral analysis presented in Soria & Kong (2002) by co-adding the pn and

MOS data (thus increasing the significance of possible line features), with a program written by M. Page, and by using updated response matrices and more recent calibration files in the SAS. The combined EPIC spectrum from 2002 February is well fitted ($\chi^2_{\nu} = 30.9/36$) by a simple power law with $\Gamma \approx 1.9$, and total (Galactic plus intrinsic) absorption $n_H \approx 1.8 \times 10^{21} \text{ cm}^{-2}$ (Table 3). This corresponds to an emitted luminosity

$\approx 1.6 \times 10^{39} \text{ erg s}^{-1}$ in the 0.3–12 keV band. Adding a black-body or multicolor disk-blackbody component at $kT \approx 0.15$ keV does not improve the fit significantly ($\chi^2_\nu = 27.8/34$). An absorbed multicolor disk-blackbody model does not provide a good fit (best-fit $kT_{\text{in}} = 1.2 \pm 0.2$ keV, but $\chi^2_\nu = 47.9/36$). We also analysed the lightcurve but found no periodicity in the 1–10,000 s range. The count rate is consistent with the source being constant over the duration of the 2002 *XMM-Newton* observation. Its emitted luminosity in 2003 must be $< 5 \times 10^{37} \text{ erg s}^{-1}$ in the 0.3–12 keV band. The upper limit, at the 3- σ significance level, was estimated with the assumption of a $\Gamma = 1.9$ power-law spectrum and total $n_{\text{H}} = 1.8 \times 10^{21} \text{ cm}^{-2}$.

The other bright source in the M 74 field, CXOU J13651.1+154547, is detected in both *Chandra* and both *XMM-Newton* observations². In the first three observations it exhibited strong variability over timescales of a few thousand seconds, with flux changes as large as an order of magnitude (Krauss et al. 2003). If we assume that this source belongs to M 74 and is not a background AGN³, typical luminosities inferred from the 2001–2002 data were $\approx 5 \times 10^{38} \text{ erg s}^{-1}$ in the faint state, with peaks of up to $\approx 8 \times 10^{39}$ during the flares. Variability over shorter timescales (~ 100 s) was also observed. Spectral analysis showed that the X-ray emission was harder when the source was brighter (Krauss et al. 2003).

Data analysis for the 2003 *XMM-Newton* observation is complicated by the location of the source on a CCD gap in the pn. We eliminated the contamination of spurious events along the chip edge by extracting only "flag-0" & "pattern-0" events. Fortunately, the source is located sufficiently far away from any chip gaps in the MOS. Taking into account vignetting (the source is 5' off-axis) and the fraction of pn events lost in the chip gap, we obtained the combined EPIC lightcurve shown in Fig. 2. The observed count rate appears to be much less variable than in 2001 and 2002, with no signs of strong flares. We carried out Fourier analysis of the data but found no significant periodicity in the 1–10,000 s range.

The co-added pn and MOS spectrum can be fitted in the 0.3–12 keV band with a simple power-law with $\Gamma \approx 2.5 \pm 0.5$, absorbed by a total column density $n_{\text{H}} \approx 1.7 \times 10^{21} \text{ cm}^{-2}$ ($\chi^2_\nu = 1.16$ for 18 d.o.f.; Fig. 3 and Table 4). Adding a multicolour black-body component or using comptonized black-body models (eg, *comptt*, *bmc* or *thcomps* in XSPEC) does not significantly improve the fit. When the Comptonization model *bmc*⁴ is used, the temperature of the seed thermal component is constrained to be $\lesssim 0.26$ keV (90% confidence level). Using the

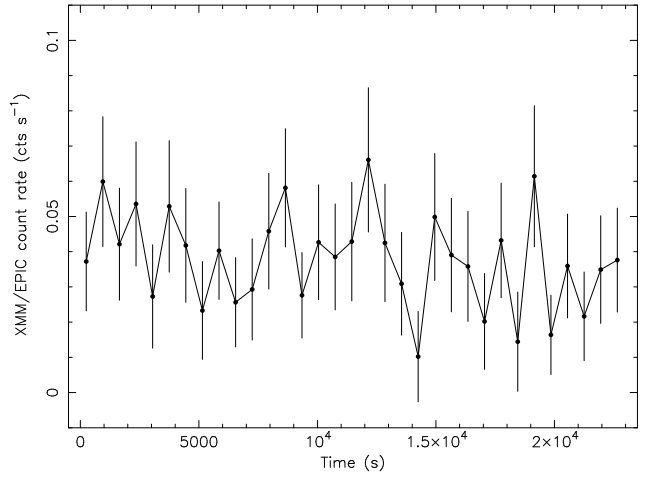


Fig. 2. Lightcurve of CXOU J13651.1+154547 for the *XMM-Newton* 2003 January observation. The data have been binned into 700 s intervals. The count rate plotted here is the total rate that would have been detected by the three EPIC instruments combined, in the 0.3–12 keV band, if the source had been observed on-axis.

Comptonization model *comptt*⁵, the seed photon temperature is $\lesssim 0.23$ keV. Finally, we checked that the observed spectrum is not consistent with an absorbed multicolor disk-blackbody ($\chi^2_\nu = 1.56$ for 18 d.o.f). Using the power-law spectral model, we obtain an emitted flux $1.3 \times 10^{-13} \text{ erg cm}^{-2} \text{ s}^{-1}$ in the 0.3–12 keV band; for the *bmc* model, the flux is $1.2 \times 10^{-13} \text{ erg cm}^{-2} \text{ s}^{-1}$. At the assumed distance of M 74, the emitted luminosity is $\approx 8 \times 10^{38} \text{ erg s}^{-1}$ for both spectral models.

As an aside, we note that XMMU J013627.2+155005 is another bright transient source seen in 2002 (when it had a hard power-law spectrum and a luminosity $\approx 3 \times 10^{38} \text{ erg s}^{-1}$, Soria & Kong 2002) but not in 2003, nor in the previous *Chandra* observations.

2.5. Colour and luminosity distribution of the other X-ray sources

In addition to an individual study of SN 2002ap, XMMU J013636.5+155036 and CXOU J013651.1+154547, we investigated the color and luminosity distribution of the discrete source population in M 74, to distinguish different physical classes of sources and estimate the relative fraction of X-ray binaries (XRBs) and supernova remnants (SNRs). The spatial resolution of the *XMM-Newton* EPIC cameras is not sufficient to resolve many faint sources in the inner disk; therefore, we used the co-added 2001 June + October *Chandra* ACIS-S observations for this study, achieving a detection limit of $\approx 10^{-4} \text{ ACIS-S cts s}^{-1}$.

Seventy-four X-ray sources (not including two obvious foreground stars) are detected with *wavdetect* at $> 3.5\sigma$ significance inside the D_{25} ellipse of M 74, in the *Chandra* ACIS-S

² This source was not discussed in Soria & Kong (2002) because in that paper we focussed only on transient sources newly detected by *XMM*

³ Two candidate “ultra-luminous” sources in the field of nearby galaxies have recently been recognised as background AGN (Masetti et al. 2003; Foschini et al. 2002). The possibility that CXOU J13651.1+154547 is a background object was discussed by Krauss et al. (2003), but considered unlikely in the absence of any radio or optical counterpart.

⁴ The *bmc* model (Shrader & Titarchuk 1999) describes the thermal or bulk motion Comptonization of a blackbody seed-photon component.

⁵ *comptt* (Titarchuk 1994) approximates the seed-photon input spectrum with the Wien tail of the blackbody spectrum. Thus, it is simpler but less accurate than the *bmc* model.

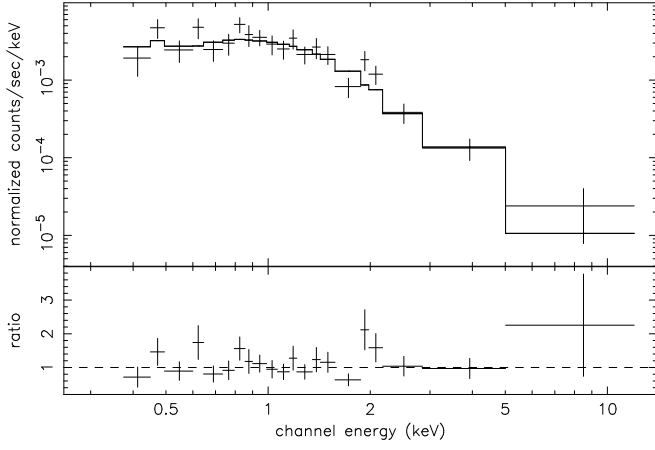


Fig. 3. Spectrum of CXOU J13651.1+154547 for the *XMM-Newton* 2003 January observation. The pn and MOS spectral data have been re-sampled and co-added to produce a combined EPIC spectrum. The background-subtracted spectrum has then been grouped to achieve a signal-to-noise ratio > 4 for each bin. The fitted model is an absorbed power-law of index $\Gamma \approx 2.5$.

Table 3. XSPEC best-fit parameters for the X-ray spectrum of XMMU J013636.5+155036 in 2002 February, from the combined *XMM-Newton* EPIC dataset. The foreground line-of-sight absorption column density $n_{\text{H,Gal}}$ has been fixed at $0.5 \times 10^{21} \text{ cm}^{-2}$. See <http://heasarc.gsfc.nasa.gov/docs/xanadu/xspec> for a full description of the XSPEC spectral models.

model: wabs _{Gal} × wabs × power-law	
$n_{\text{H}} (\times 10^{21} \text{ cm}^{-2})$	$1.3^{+0.6}_{-0.5}$
Γ	$1.91^{+0.21}_{-0.17}$
$K_{\text{pl}} (\times 10^{-5})$	$4.0^{+0.9}_{-0.7}$
χ^2_{ν} (dof)	0.86 (36)
$L_{0.3-12} (\times 10^{39} \text{ erg s}^{-1})$	$1.6^{+0.1}_{-0.3}$

image (Appendix A.1). The cumulative count rate distribution (Fig. 4) is fitted by a simple power-law of index $\alpha \approx -1.0$, for the 46 sources detected with an ACIS count rate $> 3 \times 10^{-4} \text{ cts s}^{-1}$, which we take as the completeness limit. Assuming $n_{\text{H}} = 1 \times 10^{21} \text{ cm}^{-2}$, and a power-law spectrum with $\Gamma = 1.7$, this corresponds to an emitted luminosity $\approx 2 \times 10^{37} \text{ erg s}^{-1}$. Using the results of the *Chandra* 1Ms Deep Field South exposure (Rosati et al. 2002), we estimate that as many as 20 of these 46 sources may be background AGN. We also estimate that 3 to 5 of the 11 sources detected with an ACIS count rate $> 10^{-3}$, and at most 1 of the 5 brightest sources (count rate $> 3 \times 10^{-3}$) may be from the background. After removing the estimated fraction of AGN at various fluxes, we obtain that the true slope of the cumulative count rate distribution is $\alpha \approx -0.9$

Table 4. XSPEC best-fit parameters for CXOU J13651.1+154547 in 2003 January, from the combined *XMM-Newton* EPIC dataset. $n_{\text{H,Gal}} \equiv 0.5 \times 10^{21} \text{ cm}^{-2}$ as in Table 3.

model: wabs _{Gal} × wabs × power-law	
$n_{\text{H}} (\times 10^{21} \text{ cm}^{-2})$	$1.2^{+0.9}_{-0.8}$
Γ	$2.46^{+0.47}_{-0.41}$
$K_{\text{pl}} (\times 10^{-5})$	$2.5^{+1.1}_{-0.7}$
χ^2_{ν} (dof)	1.16 (18)
$L_{0.3-12} (\times 10^{38} \text{ erg s}^{-1})$	$8.0^{+2.8}_{-3.8}$
model: wabs _{Gal} × wabs × bmc	
$n_{\text{H}} (\times 10^{21} \text{ cm}^{-2})$	$1.2^{+4.3}_{-1.2}$
$T_{\text{bb}} (\text{keV})$	$0.13^{+0.13}_{-0.13}$
Γ	$2.22^{+0.82}_{-1.22}$
$K_{\text{bmc}} (\times 10^{-7})$	$9.2^{+5.0}_{-5.0}$
χ^2_{ν} (dof)	1.25 (16)
$L_{0.3-12} (\times 10^{38} \text{ erg s}^{-1})$	$7.7^{+1.2}_{-3.0}$

($\alpha \approx -0.8$ for sources more luminous than $\approx 10^{38} \text{ erg s}^{-1}$; this is in agreement with the slope found by Soria & Kong (2002)).

A power-law luminosity function is consistent with the distribution observed in disks of other spiral galaxies with moderately active star formation (eg, $\alpha \approx -0.8$ in M 101, see Pence et al. 2001; $\alpha \approx -1.1$ – -0.9 in the disk of M 31, see Kong et al. 2003). A steeper power-law index ($\alpha \approx -1.7$) is generally observed in spiral bulges, which are dominated by old stellar populations, while flatter slopes ($\alpha \approx -0.5$) are typical of starburst galaxies (eg, the Antennae and M 82; see Zezas & Fabbiano 2002 and references therein).

Colour-colour plots (Figs. 4 and 5) are an effective way of separating the discrete sources into separate physical groups: soft and hard XRBs, SNRs and supersoft sources. We chose the colour indices $[(H - M)/(H + M + S), (M - S)/(H + M + S)]$, following Prestwich et al. (2003). The spectral models overplotted in the diagrams are: power-laws with photon indices $\Gamma = 1.3$, $\Gamma = 1.7$ and $\Gamma = 2.0$ (characteristic of XRBs in the hard state); disk-blackbody with inner-disk temperatures $kT_{\text{in}} = 0.5 \text{ keV}$ and $kT_{\text{in}} = 1.0 \text{ keV}$ (typical of XRBs in the soft state); optically-thin, single-temperature thermal plasma at $kT_{\text{rs}} = 0.5 \text{ keV}$ (typical of SNRs); blackbody at $kT_{\text{bb}} = 0.1 \text{ keV}$ (typical of supersoft sources). Along each model line, the column density increases from the bottom to the top (models 1 and 2) or clockwise (models 3–7): from $n_{\text{H}} = 5 \times 10^{20} \text{ cm}^{-2}$ (line-of-sight foreground absorption for M 74) to $n_{\text{H}} = 5 \times 10^{21} \text{ cm}^{-2}$ for the blackbody model, to $n_{\text{H}} = 7.5 \times 10^{21} \text{ cm}^{-2}$ for the optically-thin thermal plasma model, to $n_{\text{H}} = 2 \times 10^{22} \text{ cm}^{-2}$

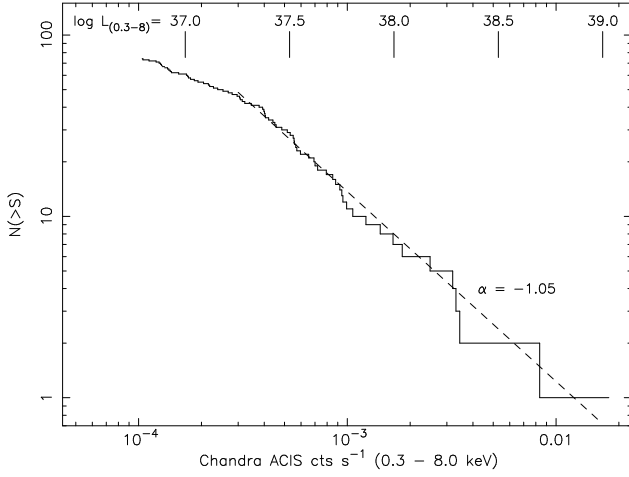


Fig. 4. Cumulative count-rate distribution (“luminosity function”) for the 74 sources found inside the D_{25} ellipse in the combined *Chandra* observations. For each source, the count rate plotted here is the average of the 2001 June and October count rates. Two obvious foreground stars are not included. See Sect. 2.5 for an estimate of the background AGN contribution.

for the disk-blackbody models, and to $n_H = 5 \times 10^{22} \text{ cm}^{-2}$ for the power-law models. In calculating the expected colours for each of those spectral models, we took into account the time-dependent degradation of the ACIS detector at soft channel energies.

We also plotted in Figs. 5 and 6 the approximate colours that SN 2002ap would have had if it had been observed with the ACIS-S detector⁶. The source colours fall in the region of the diagram which in star-forming galaxies is usually populated by thermal SNRs (eg, Prestwich et al. 2003; Soria & Wu 2003; Soria & Kong 2003).

3. Discussion

3.1. The X-ray behaviour of SN 2002ap

Type Ib/c SNe are rare occurrences in nearby galaxies, and they are only rarely observed in the X-rays. It is not clear whether there is a “typical” X-ray behaviour. In fact, the two best-monitored previous cases of Type Ic X-ray SNe, 1994I and 1998bw, have substantially different X-ray light curves at early times (Fig. 7). SN 1998bw exhibited early X-ray emission (detected by *BeppoSAX*) in the 0.1–10 keV range, starting 10 hours after the explosion (Pian et al. 2000). The initial decline was slow: only a factor ≈ 2.5 over the first 6 months. An *XMM-Newton* measurement nearly 4 years later shows that the X-ray decline must have been faster at later epochs (Fig. 7;

⁶ The conversion between the *XMM-Newton* and *Chandra* count rates in the three bands depends of course on the assumed spectral model and absorption, but these variations are small for the range of column densities and temperatures considered in Table 2. We converted the colours using the correct response matrices generated by the CIAO and SAS software, rather than the default (pre-launch) responses from PIMMS.

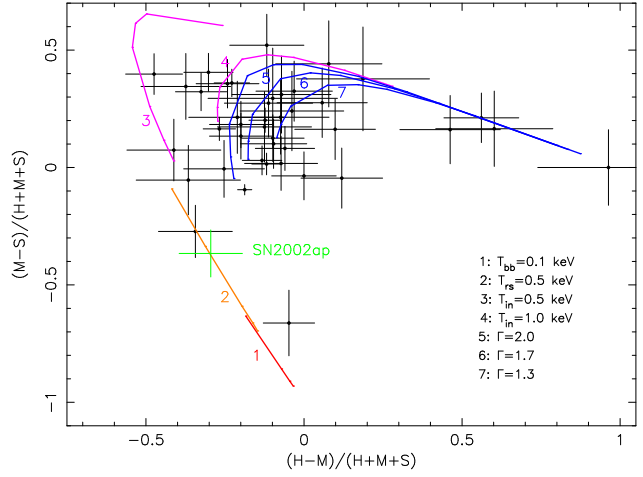


Fig. 5. X-ray colour-colour plot of the 46 brightest sources (those with an average count rate $> 3 \times 10^{-4} \text{ cts s}^{-1}$) found inside the D_{25} ellipse of M 74 in the two *Chandra* observations. The three bands are: $S = 0.3\text{--}1.0 \text{ keV}$; $M = 1.0\text{--}2.0 \text{ keV}$; $H = 2.0\text{--}8.0 \text{ keV}$. We overplotted the expected colours for some basic spectral models, which help us separate the different physical classes of sources. Along each model curve, the absorbing column density increases from the bottom to top (models 1–2) or clockwise (models 3–7). For comparison, we also plotted the approximate colour that SN 2002ap would have had in 2002 February if it had been observed by *Chandra* ACIS-S3.

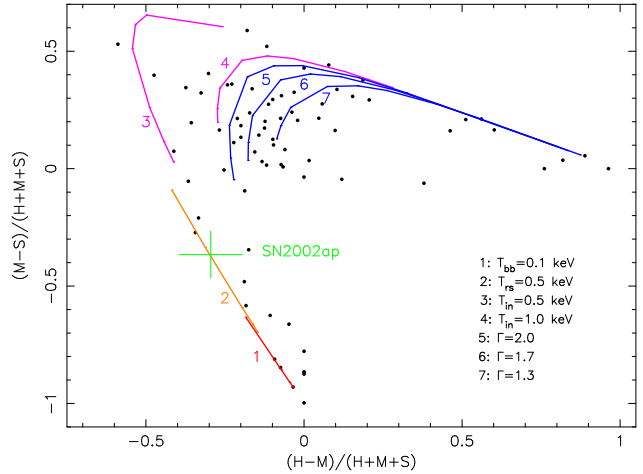


Fig. 6. X-ray colour-colour plot of all the sources found inside the D_{25} ellipse of M 74 in the two *Chandra* observations, without error bars. The three energy bands and the spectral models have been chosen like in Fig. 5.

Pian et al. 2003). In contrast, SN 1994I was not detected by *ROSAT* until day 82 after the explosion (Immler et al. 1998). However, its late-epoch temporal behaviour (i.e. after day 82), sampled by *Chandra* (Immler et al. 2002), is consistent with that of SN 1998bw (Fig. 7).

The temporal behaviour of SN 2002ap is overall more similar to that of SN 1998bw, in the sense that both SNe showed

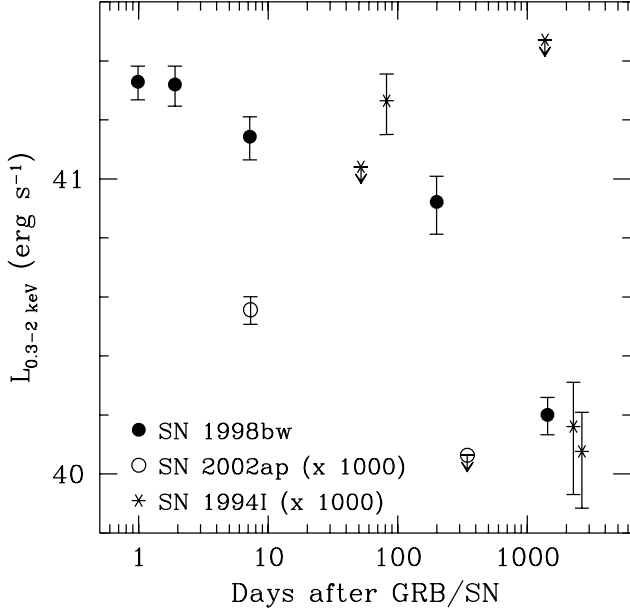


Fig. 7. The lightcurves of Type Ic SNe 1998bw, 1994I and 2002ap in the 0.3–2 keV band. The datapoints for SN 1998bw and SN 1994I are taken from Pian et al. (2003) and references therein, and from Immler et al. (2002), respectively.

prompt X-ray emission. The 2003 upper limit on the X-ray flux of SN 2002ap is at least 7 times fainter than the 2002 detection: this is roughly consistent with the decay rate of SN 1998bw (Fig. 7). The early X-ray detection of SN 1998bw may suggest the presence of a jet, in which prompt, non-thermal radiation can be efficiently produced, similar to GRB afterglow radiation (see Pian et al. 2003). However, the absence of hard X-ray emission in SN 2002ap (the upper limit on the 2–12 keV flux implies a luminosity at least a factor ~ 1000 lower than in SN 1998bw) argues against the presence of highly relativistic conditions at the forward (circumstellar) shock. This SN was also less radio-luminous than SN 1998bw (Berger et al. 2002). The lower energy emitted in the X-ray and radio bands is consistent with the estimate of the total energy of SN 2002ap (5×10^{51} erg s^{-1}), which is an order of magnitude smaller than in SN 1998bw (Mazzali et al. 2002). While the consistency of the temporal X-ray behaviour of SN 2002ap with that of SN 1998bw could support its classification as a hypernova, suggested on the basis of optical observations (Mazzali et al. 2002; Foley et al. 2003), the lower total energy may be insufficient for the development of a strongly asymmetric explosion, as required for the formation of a GRB. Indeed, a search for gamma-ray signal during the week prior to the SN 2002ap explosion resulted in no detection (Hurley et al. 2002).

X-ray emission from a SN may originate either from the forward shock or from the reverse shock (eg, Immler & Lewin 2002 and Chevalier & Fransson 2002 for reviews). Following the self-similar analytical approximation of Fransson et al. (1996), and of Chevalier & Fransson (1994),

one can parameterise the radial density profile ρ of the ejecta as a function of time t , as $\rho = Kt^{-3}(r/t)^{-n}$, where: r is the radial distance from the centre of the progenitor; the proportionality constant K depends on the velocity V of the ejecta at the reverse shock (maximum velocity of the ejecta at any given time); the choice of the power-law index n depends on the type of progenitor star. The circumstellar wind density ρ_w can be parameterised as:

$$\rho_w = \frac{\dot{M}}{4\pi v_w r_0^2} \left(\frac{r_0}{r} \right)^s \quad (1)$$

where r_0 is a reference radius corresponding to the mass-loss rate \dot{M}/v_w ($r_0 = 10^{15}$ cm in Fransson et al. 1996), and $1.5 \lesssim s \lesssim 2$ (Fransson et al. 1996). The mass-loss rate $\dot{M} \approx 5 \times 10^{-7} M_\odot$ yr^{-1} for the progenitor of SN 2002ap (Berger et al. 2002). The stellar-wind velocity v_w is generally of the same order as the escape velocity from the progenitor star, that is $\sim 10^3$ km s^{-1} in the case of Type Ic SN progenitors. As noted earlier, the low radio and hard X-ray luminosities of SN 2002ap seem to rule out a relativistic speed for the ejecta: it is more likely that $V \sim (1-3) \times 10^4$ km s^{-1} , as is the case in most core-collapse SNe (eg, Matzner & McKee 1999).

In the thin shell approximation, and assuming electron-ion equipartition, the forward shock has a temperature

$$kT_f \approx 196 \mu_s \left(\frac{n-3}{n-s} \right)^2 V_4^2 \text{ keV} \approx 150 V_4^2 \text{ keV}, \quad (2)$$

where $V_4 \equiv V/(10^4 \text{ km } s^{-1})$, and μ_s is the mean mass per particle. μ_s is a function of chemical abundance: $\mu_s = 0.61$ for solar abundance, and, more generally, $0.5 < \mu_s \lesssim 1$. We have also assumed $n \gg 3$, $n \gg s$ (Fransson et al. 1996). The temperature of the reverse shock is (Fransson et al. 1996):

$$kT_r = \left(\frac{3-s}{n-3} \right)^2 kT_f = 196 \mu_s \left(\frac{3-s}{n-s} \right)^2 V_4^2 \text{ keV}. \quad (3)$$

The observed colours of SN 2002ap imply temperatures $0.5 \lesssim kT \lesssim 0.9$ keV, suggesting that the emission comes from the reverse shock, and that the density gradient of the ejecta is very steep, with $n \gtrsim 20$, from Eq.(3).

The cooling timescale t_{cool} of the reverse shock, at each time t after the SN event, depends on n , s , V , \dot{M} and v_w (Equation (3.14) in Fransson et al. 1996). Taking $s = 2$, and $t = 5$ d (time of the *XMM-Newton* observation), one obtains:

$$t_{cool} = 1.5 \times 10^7 \frac{V_4^{5.34}}{(n-3)(n-4)(n-2)^{3.34}} \frac{v_{w,3}}{\dot{M}_{-6}} \text{ d}, \quad (4)$$

where \dot{M}_{-6} is the mass-loss rate in units of $10^{-6} M_\odot$ yr^{-1} , and $v_{w,3}$ the wind speed in units of 10^3 km s^{-1} . For $n \gtrsim 20$, and $v_{w,3}/\dot{M}_{-6} \approx 1$, $t_{cool} \approx 10^7 (V_4/n)^{5.34}$ d, i.e., only a few days or weeks. We would not expect the reverse shock to remain radiative after a year.

The total luminosity emitted by the reverse shock is (for $s = 2$):

$$L_r = 1.6 \times 10^{38} V_4^3 \frac{(n-3)(n-4)}{(n-2)^3} \frac{\dot{M}_{-6}}{v_{w,3}} \text{ erg } s^{-1}. \quad (5)$$

This simple approximation gives an emitted luminosity $\sim 10^{37}$ erg s $^{-1}$, in agreement with the observations (Table 2) if the absorbing column density is $\lesssim 10^{21}$ cm $^{-2}$. On the other hand, the same model predicts an X-ray luminosity from the forward shock $\sim 10^{31}$ – 10^{32} erg s $^{-1}$, entirely negligible (Fransson et al. 1996). As the reverse shock cools down radiatively, a cold shell is formed between the reverse shock and the contact discontinuity, with a column density that scales $\sim (n - 4)(Vt)^{-1}(\dot{M}/v_w)$ (Fransson et al. 1996). At $t = 5$ d after the event, and for values of the physical parameters suitable to SN 2002ap, this implies an intrinsic column density $\approx (1-2) \times 10^{20}$ cm $^{-2}$.

In conclusion, we argue that the low temperature ($kT \approx 0.8$ keV) of the X-ray emission observed from SN 2002ap on 2002 February 2 points to a radiatively-cooling reverse shock as the origin of the X-rays. If so, the fact that it was already detected 5 d after the event implies that the cool shell between the reverse shock and the contact discontinuity was already optically thin. The ratio of mass-loss rate over stellar-wind velocity is the crucial factor determining the column density across the cool shell (scaling as (\dot{M}/v_w)) and the luminosity of the forward shock (scaling as $(\dot{M}/v_w)^2$). For Type Ic SNe, which originate from a massive but more compact progenitor, this factor may be $\sim 10^3$ times smaller than for Type II SNe (eg, SN 1993J; SN 1999em). Hence, in the latter cases the cool shell is generally optically thick to the soft X-ray emission until a few weeks or months after the event (Fransson et al. 1996; Immler & Lewin 2002), and only hard X-ray emission from the forward shock may be detected in the initial phases. In this scenario, the late X-ray detection of SN 1994I suggests a higher \dot{M}/v_w ratio for this object (Immler et al. 2002), than for SN 1998bw and SN 2002ap, despite all three being classified as Type Ic events.

The limited S/N and the scarce temporal information do not allow us to measure the X-ray flux decline timescale in SN 2002ap, and therefore we are unable to investigate in more detail the density of the circumstellar medium as a function of radial distance from the SN, and the cooling timescale of the shocked ejecta. More cases of Type Ic SNe must be followed with *XMM-Newton*, to understand the emission processes, constrain the parameters of the circumstellar medium and detect possible deviations from isotropy in the geometry of the explosion.

3.2. Nature of the brightest X-ray sources

Accreting X-ray sources are usually classified as “ultra-luminous” (ULXs) when they are persistently brighter than the “classical” Eddington limit of a $\approx 7M_\odot$ BH (eg, Colbert & Mushotzky 1999; Roberts & Warwick 2000; Makishima et al. 2000). In 2002 February, XMMU J013636.5+155036 was the brightest source in M 74 with a luminosity $\approx 1.6 \times 10^{39}$ erg s $^{-1}$, approximately constant over the 25-ks observation, and a featureless power-law X-ray spectrum. Its location in a star-forming region suggested that the source was a high-mass X-ray binary. However, the source was no longer detected in 2003, its flux having declined by at least 30 times, and we cannot determine how long the high state may have lasted.

Repeated observations in the future will be necessary to determine its duty cycle.

The other candidate ULX in M 74, CXOU J013651.1+154547, showed little variability in the 2003 January observation, at a luminosity of $\approx 8 \times 10^{38}$ erg s $^{-1}$. The persistent component of the X-ray emission was $\approx 5 \times 10^{38}$ erg s $^{-1}$ in 2001 October and 2002 February (Krauss et al. 2003). Hence, the “steady” X-ray luminosity appears to be always less than the Eddington limit for a “canonical” $7M_\odot$ BH. (This is still the case even for the larger distance to M 74 assumed by Krauss et al. 2003). The new observation suggests that the X-ray spectrum in the non-flaring state is marginally softer than during flares, and that it is dominated by the non-thermal (power-law) component, usually interpreted as Compton-scattered emission. Any additional blackbody or disk-blackbody components (required to provide the soft seed photons) are constrained to have temperatures $\lesssim 0.25$ keV. If confirmed, such a low temperature is consistent with a standard geometrically-thin accretion disk around an intermediate-mass BH (Makishima et al. 2000). Alternatively, it would also be consistent with thermal emission from Compton-thick outflows (King & Pounds 2003) which may occur for super-Eddington accretion rates ($\dot{M} > \dot{M}_{\text{Edd}}$).

In the first three observations, hard X-ray flares were detected on top of the persistent component, on timescales of a few thousand seconds. During the flares, the source exceeded the $7M_\odot$ Eddington limit by up to a factor of 10, but only for short periods of time: none of the flares lasted longer than ≈ 1 h. The rapid variability was interpreted (Krauss et al. 2003) as evidence of a beamed emission component, possibly associated with a jet. It may not be necessary to invoke a micro-quasar scenario to explain the flares: short episodes of super-Eddington emission are sometimes also found in neutron-star XRBs. For example, the high-mass XRB LMC X-4 shows a persistent luminosity $\approx 2 \times 10^{38}$ erg s $^{-1} \approx L_{\text{Edd}}$ for a neutron star, with repeated bursts/flares (typical duration ~ 100 s) reaching peak luminosities $\approx 2 \times 10^{39}$ erg s $^{-1}$ (Moon et al. 2003). The “Rapid Burster” MXB 1730–335 and GRO J1744–28 are two other examples of rapid, repeated flaring (Lewin et al. 1996). The X-ray bursts in these systems are generally thought to be caused by the spasmodic release of gravitational potential energy (“Type-II” bursts, as opposed to the thermo-nuclear “Type-I” bursts; eg, Lewin 1995). However, the exact mechanism is still unclear and may differ from source to source. Thermal-viscous instabilities in the inner disk region have been invoked to explain the inhomogeneous accretion (Cannizzo 1996, 1997). Alternatively, the flares have been attributed to the accumulation and subsequent sudden release of accreting matter at a centrifugal barrier; in the case of a neutron star, the barrier can be created by the magnetosphere of the rapidly rotating compact object (Bann 1977, 1979). Mass transfer instabilities or inhomogeneous winds from the companion star have also been suggested (Vogt & Penrod 1983). Further X-ray studies of CXOU J013651.1+154547 will be required to ascertain whether its flaring behaviour could be an example of Type-II bursts in a stellar-mass BH XRB, and to determine what physical mechanism is responsible for the intermittent ac-

cretion, or for the intermittent ejections in the micro-quasar scenario.

3.3. X-ray colours of the point sources

The discrete X-ray sources are roughly clustered into three main groups in the colour-colour plots (Figs. 5 and 6). Firstly, “classical” supersoft sources have detectable emission only in the soft band and are therefore located at $(H-M)/(S+M+H) \approx 0$, $(M-S)/(S+M+H) \lesssim -0.7$. Secondly, a group of soft sources with detectable emission in the soft and medium band is located at $-0.7 \lesssim (M-S)/(S+M+H) \lesssim -0.2$. It has been suggested (Prestwich et al. 2003) that thermal SNRs dominate this class of sources. Thirdly, most XRBs have $-0.2 \lesssim (M-S)/(S+M+H) \lesssim 0.5$, with a broad spread in $(H-M)/(S+M+H)$. (See also Soria & Wu (2003) and Soria & Kong (2003) for a discussion of colour-colour plots in other nearby spiral galaxies, and Di Stefano & Kong (2003) for a classification of soft and supersoft sources.) A preliminary comparison between the two *Chandra* and two *XMM-Newton* observations shows that at least three bright ($\sim 10^{38} \text{ erg s}^{-1}$) candidate XRBs exhibit spectral transitions between a harder and a softer state. This is beyond the scope of this paper and is left to further work.

Above our detection limit of $\approx 10^{-4} \text{ ACIS-S cts s}^{-1}$ ($L_x \approx 6 \times 10^{36} \text{ erg s}^{-1}$ for the spectral model assumed in Sect. 2.5), 7 out of the 74 point sources are supersoft ($kT \lesssim 100 \text{ eV}$), another 7 are in the soft subgroup. Of the remaining 60 sources, about half are XRBs and the other half are likely to be background AGN. Hence, supersoft sources represent about 15% of the true galactic sources brighter than our detection limit, and soft sources another 15%. Among the sources brighter than $3 \times 10^{-4} \text{ ACIS-S cts s}^{-1}$, none are supersoft, 2 are soft and 44 are consistent with XRB colours (20 of them may be AGN). Hence, the fraction of soft sources is less than 8%, much lower than in more actively star-forming late-type spiral galaxies. For example, we can compare M 74 with M 83 (Soria & Wu 2003), taking into account that the distance to M 83 is $\approx 1/2$ of the distance to M 74 (de Vaucouleurs et al. 1991; Thim et al. 2003). In M 83, soft sources represent more than 40% of the X-ray point sources brighter than what would be the detection limit in our M 74 study, and 25% of the sources in the brighter subgroup. This is consistent with the interpretation of the soft sources as candidate X-ray SNRs: the number of detected SNRs at a given luminosity is related to the recent star-formation rate in a galaxy, as well as to other factors such as the density of the interstellar medium. A more comprehensive study of these issues is left to further work.

4. Conclusion

We investigated the X-ray source population in the late-type spiral M 74. We took a new *XMM-Newton* observation in 2003 January to study the evolution of the rare Type Ic SN 2002ap a year after the event, and monitor the variability of two bright BH candidates. In addition, we used archival *Chandra* ACIS observations from 2001 June and October to determine the

luminosity and colour distribution of all the other discrete sources.

We have more accurately determined the X-ray colours and luminosity of SN 2002ap five days after the event, and put an upper limit to its luminosity a year later. Unlike other well-studied core-collapse SNe (eg, SN 1999em: Pooley et al. 2002), SN 2002ap was not dominated by hard X-ray emission in its early stages. The X-ray colours observed in 2002 February were soft, suggesting that the dominant component was optically-thin thermal emission at $kT < 1 \text{ keV}$. Assuming an absorbing column density $\lesssim 10^{21} \text{ cm}^{-2}$, we estimate an emitted luminosity of $\approx 5 \times 10^{37} \text{ erg s}^{-1}$ in the 0.3–12 keV band, on 2002 February 2. The emitted luminosity in the 2–12 keV band is at least an order of magnitude lower. After 11 months, the source was no longer detected, implying that its luminosity had decreased by at least a factor of seven. We argue that the prompt soft X-ray emission was coming from the reverse shock, and that this is consistent with a low mass-loss rate and high stellar-wind velocity from the progenitor, as expected in Type Ic events. Unlike for other Type Ic events such as SN 1998bw, there is no evidence of relativistic ejecta.

Seventy-four discrete X-ray sources (not including two obvious foreground stars) were detected inside the D_{25} ellipse in the combined *Chandra* observations, with a detection limit of $\approx 6 \times 10^{36} \text{ erg s}^{-1}$ (completeness limit $\approx 2 \times 10^{37} \text{ erg s}^{-1}$). After subtracting the estimated background AGN contribution, the luminosity distribution of the discrete sources is well modelled by a simple power-law of slope ≈ -0.9 , similar to the value inferred for other moderately active star-forming spiral disks. About 15% of the true M 74 sources have soft colors consistent with thermal SNRs: they are all fainter than a *Chandra* ACIS-S count rate of $\approx 5 \times 10^{-4} \text{ cts s}^{-1}$, corresponding to emitted luminosities $\approx 2 \times 10^{37} \text{ erg s}^{-1}$ (for a $kT = 0.6 \text{ keV}$ thermal plasma model and $n_H = 10^{21} \text{ cm}^{-2}$). All brighter sources are likely XRBs.

We have studied the temporal and spectral behaviour of the two brightest X-ray sources previously found in M 74. XMMU J013636.5+155036 (emitted luminosity $\approx 1.6 \times 10^{39} \text{ erg s}^{-1}$ in 2002) is no longer detected in 2003 and must now be fainter than $5 \times 10^{37} \text{ erg s}^{-1}$. The flaring source CXOU J013651.1+154547 has settled into a soft state: its power-law spectrum has photon index $\Gamma \approx 2.5$; any additional thermal component is constrained to temperatures $\lesssim 0.25 \text{ keV}$. Its luminosity shows only little variations around an average value $\approx 8 \times 10^{38} \text{ erg s}^{-1}$. In the 21 ks of our 2003 January observation we did not find any of the hard flares (peak luminosity $\approx 10^{40} \text{ erg s}^{-1}$) detected in 2001–2002 (Krauss et al. 2003). The nature of the super-Eddington bursts remains unclear: we argue that they could either be due to beamed emission in a microquasar/jet scenario (as proposed by Krauss et al. 2003), or be analogous to Type-II bursts in neutron star XRBs, ie due to episodes of spasmodic/intermittent accretion in addition to a steady sub-Eddington component.

Acknowledgements. We thank Norbert Schartel for his assistance in the *XMM-Newton* ToO observation, Miriam Krauss for sending us her latest preprint, Mat Page and Kinwah Wu for useful discussions, and an anonymous referee for his/her suggestions.

References

- Arnaud, K. A. 1996, *Astronomical Data Analysis Software and Systems V*, eds. G. Jacoby and J. Barnes, ASP Conference Series Volume 101, p. 17
- Berger, E., Kulkarni, S. R., & Chevalier, R. A. 2002, *ApJ*, 577, L5
- Bann, W. A. 1977, *ApJ*, 214, 245
- Bann, W. A. 1979, *ApJ*, 227, 987
- Boles, T., Schwartz, M., Swift, B., & Li, W. 2003, *IAU Circ.* 8048
- Bottinelli, L., Gouguenheim, L., Paturel, G., & de Vaucouleurs, G. 1984, *A&AS*, 56, 381
- Cannizzo, J. K. 1996, *ApJ*, 466, L31
- Cannizzo, J. K. 1997, *ApJ*, 482, 178
- Chevalier, R. A., & Fransson, C. 2002, in "Supernovae and Gamma-Ray Bursts," ed. K. W. Weiler (Springer-Verlag), astro-ph/0110060
- Colbert, E. J. M., & Mushotzky, R. F. 1999, *ApJ*, 519, 89
- de Vaucouleurs, G., de Vaucouleurs, A., Corwin, H. Jr., et al. 1991, *Third Reference Catalogue of Bright Galaxies*, (Springer-Verlag, New York)
- Dickey, J. M., & Lockman, F. J. 1990, *ARAA*, 28, 215
- Di Stefano, R., & Kong, A. K. H. 2003, *ApJ*, in press (astro-ph/0301162)
- Foley, R. J., Papenkova, M. S., Swift, B. J., et al. 2003, *PASP*, in press (astro-ph/0307136)
- Foschini, L., Ho, L. C., Masetti, N., et al. 2002, *A&A*, 396, 787
- Fox, D. W., & Lewin, W. H. G. 1999, *IAU Circ.* 7318
- Fox, D. W., Lewin, W. H. G., Fabian, A., et al. 2000, *MNRAS*, 319, 1154
- Fransson, C., Lunqvist, P., & Chevalier, R. A. 1996, *ApJ*, 461, 993
- Galama, T., Vreeswijk, P. M., van Paradijs, J., et al. 1998, *Nature*, 395, 670
- Huchra, J. P., Vogeley, M. S., & Geller, M. J. 1999, *ApJS*, 121, 287
- Hurley, K., Mazets, E., Golenetskii, S., et al. 2002, *GCN* 1252⁷
- Immler, S., Aschenbach, B., & Wang, Q. D. 2001, *ApJ*, 561, L107
- Immler, S., & Lewin, W. H. G. 2002, in "Supernovae and Gamma-Ray Bursts," ed. K. W. Weiler (Springer-Verlag), astro-ph/0202231
- Immler, S., Pietsch, W., & Aschenbach, B. 1998, *A&A*, 336, L1
- Immler, S., Wilson, A. S., & Terashima, Y. 2002, *ApJ*, 573, L27
- Inoue, H., Hayashida, K., Itoh, M., et al. 1991, *PASJ*, 43, 213
- Iwamoto, K., Mazzali, P. A., Nomoto, K., et al. 1998, *Nature*, 395, 672
- Kennicutt, R. C., & Hodge, P. W. 1980, *ApJ*, 241, 573
- King, A. R., & Pounds, K. A. 2003, *MNRAS*, in press (astro-ph/0305541)
- Kong, A. K. H., Di Stefano, R., Garcia, M. R., & Greiner, J. 2003, *ApJ*, 585, 298
- Krauss, M. I., Kilgard, R. E., Garcia, M. R., Roberts, T. P., & Prestwich, A. H. 2003, *ApJ*, submitted
- Kulkarni, S. & Fox, D. W. 2003, *IAU Circ.* 8073
- Leising, M. D., Kurfess, J. D., Clayton, D. D., et al. 1994, *ApJ*, 431, L95
- Lewin, W. H. G. 1995, in *X-Ray Binaries*, ed. W. H. G. Lewin, J. van Paradijs, & E. van den Heuvel (Cambridge: Cambridge Univ. Press)
- Lewin, W. H. G., Rutledge, R. E., Kommers, J. M., van Paradijs, J., & Kouveliotou, C. 1996, *ApJ*, 462, L39
- MacFadyen, A. I., & Woosley, S. E. 1999, *ApJ*, 524, 262
- Makishima, K., Kubota, A., Mizuno, T., et al. 2000, *ApJ*, 535, 632
- Masetti, N., Foschini, L., Ho, L. C., et al. 2003, *A&A*, in press (astro-ph/0305452)
- Matheson, T., Challis, P., Kirshner, R. P., & Garnavich, P. M. 2003, *GCN* 1846
- Matzner, C. D., & McKee, C. F. 1999, *ApJ*, 510, 1999
- Mazzali, P. A., Deng, J., Maeda, K., et al. 2002, *ApJ*, 572, L61
- Moon, D.-S., Eikenberry, S. S., & Wasserman, I. M. 2003, *ApJ*, 586, 1280
- Paczynski, B. 1998, *ApJ*, 494, L45
- Pence, W. D., Snowden, S. L., Mukai, K., Kuntz, K. D. 2001, *ApJ*, 561, 189
- Pian, E., Amati, L., Antonelli, L. A., et al. 2000, *ApJ*, 536, 778
- Pian, E., Giommi, P., Amati, L., et al. 2003, *Adv. Sp. Res.* (Proceedings of the 34th COSPAR Scientific Assembly, Houston, 10-19 October 2002), in press, astro-ph/0304521
- Pooley, D., Lewin, W. H. G., Fox, D. W., et al. 2002, *ApJ*, 572, 932
- Pooley, D., & Lewin, W. H. G. 2002, *IAU Circ.* 8024
- Predehl, P., & Schmitt, J. H. M. M. 1995, *A&A*, 293, 889
- Prestwich, A. H., Irwin, J. A., Kilgard, R. E., et al. 2003, *ApJ*, submitted (astro-ph/0206127)
- Roberts, T. P., & Warwick, R. S. 2000, *MNRAS*, 315, 98
- Rosati, P., Tozzi, P., Giacconi, R., et al. 2002, *ApJ*, 566, 667
- Sandage, A., & Tammann, G. A. 1974, *ApJ*, 191, 603
- Schlegel, D. J., Finkbeiner, D. P., & Davis, M. 1998, *ApJ*, 500, 525
- Schlegel, E. M. 1995, *Rep. Prog. Phys.*, 58, 1375
- Schlegel, E. M. 1999, *ApJ*, 527, L85
- Schlegel, E. M. 2001, *ApJ*, 556, L25
- Schlegel, E. M. 2002, *IAU Circ.* 7913
- Sharina, M. E., Karachentsev, I. D., & Tikhonov, N. A. 1996, *A&AS*, 119, 499
- Shostak, G. S., & van der Kruit, P. C. 1984, *A&A*, 132, 20
- Shrader, C. R., & Titarchuk, L. 1999, *ApJ* 521, L21
- Sohn, Y.-J., & Davidge, T. J. 1996, *AJ*, 111, 2280
- Soria, R. & Kong, A. 2002, *ApJ*, 572, L33
- Soria, R. & Kong, A. K. H. 2003, *A&A*, submitted
- Soria, R. & Wu, K. 2003, *A&A*, in press (astro-ph/0307217)
- Sunyaev, R., Kaniovsky, A., Efremov, V., et al. 1987, *Nature*, 330, 227
- Sutaria, F. K., Chandra, P., Bhatnagar, S., & Ray, A. 2003, *A&A*, 397, 1011
- Takada-Hidai, M., Aoki, W., & Zhao, G. 2002, *PASJ*, 54, 899
- Thim, F., Tammann, G. A., Saha, A., et al. 2003, *ApJ*, in press (astro-ph/0303101)
- Titarchuk, L. 1994, *ApJ*, 434, 570
- Vogt, S. S., & Penrod, G. D. 1983, *ApJ*, 275, 661
- Zezas, A., & Fabbiano, G. 2002, *ApJ*, 577, 726
- Zimmermann, H.-U., & Aschenbach, B. 2003, *A&A* in press (astro-ph/0304322)

Appendix A: *Chandra* source list and count rates

⁷ The GCN archive is at http://gcn.gsfc.nasa.gov/gcn3_archive.html.

Table A.1. Source ID and average count rates (total and in three narrow bands) of the discrete X-ray sources detected by *Chandra* ACIS-S in the combined 2001 June–October observation. The count rates are in units of 10^{-4} cts s^{-1} . Errors are 1σ , with 3σ upper limits for sources not detected in a certain band.

IAU Name	Count rate (0.3 – 8) keV	Count rate (0.3 – 1) keV	Count rate (1 – 2) keV	Count rate (2 – 8) keV
CXOU J013623.5 + 154458	5.7 ± 1.2	0.8 ± 0.4	2.3 ± 0.7	1.8 ± 0.6
CXOU J013623.6 + 154309	8.5 ± 1.5	1.3 ± 0.4	4.0 ± 1.0	3.4 ± 0.9
CXOU J013625.1 + 154859	17.9 ± 1.4	2.9 ± 0.6	10.1 ± 1.1	4.7 ± 0.7
CXOU J013626.6 + 154458	1.9 ± 0.5	0.6 ± 0.1	0.7 ± 0.3	0.5 ± 0.2
CXOU J013626.7 + 154304	5.6 ± 1.2	0.1 ± 0.1	2.2 ± 0.7	3.2 ± 0.9
CXOU J013627.8 + 154752	33.4 ± 1.9	12.1 ± 1.2	12.6 ± 1.2	8.7 ± 1.0
CXOU J013628.7 + 154859	1.7 ± 0.5	0.1 ± 0.1	0.1 ± 0.1	1.1 ± 0.4
CXOU J013629.0 + 154319	1.2 ± 0.4	0.2 ± 0.1	0.5 ± 0.2	0.5 ± 0.2
CXOU J013629.5 + 154656	4.3 ± 0.7	< 0.1	< 0.1	4.3 ± 0.7
CXOU J013630.0 + 154855	3.2 ± 0.6	2.5 ± 0.5	0.6 ± 0.2	< 0.1
CXOU J013630.1 + 154520	8.5 ± 1.0	0.2 ± 0.1	4.7 ± 0.7	3.7 ± 0.7
CXOU J013630.4 + 154519	9.4 ± 1.1	2.7 ± 0.6	3.9 ± 0.7	2.9 ± 0.6
CXOU J013631.1 + 154458	4.5 ± 0.8	< 0.1	1.9 ± 0.5	2.2 ± 0.5
CXOU J013631.7 + 154848	15.2 ± 1.3	3.4 ± 0.6	8.3 ± 1.0	3.4 ± 0.6
^a CXOU J013631.9 + 154507	12.2 ± 1.2	10.1 ± 1.1	1.9 ± 0.5	0.2 ± 0.1
CXOU J013635.2 + 154657	3.1 ± 0.6	0.2 ± 0.1	1.1 ± 0.4	1.8 ± 0.5
CXOU J013635.3 + 154711	4.0 ± 0.7	1.6 ± 0.4	1.9 ± 0.5	0.3 ± 0.2
CXOU J013635.3 + 154227	2.2 ± 0.6	< 0.1	0.5 ± 0.2	1.7 ± 0.5
CXOU J013635.4 + 154953	1.7 ± 0.5	0.4 ± 0.2	0.3 ± 0.1	1.0 ± 0.3
CXOU J013635.7 + 154556	7.4 ± 0.9	2.2 ± 0.5	2.9 ± 0.6	2.2 ± 0.5
CXOU J013637.5 + 155030	1.3 ± 0.4	< 0.1	0.8 ± 0.3	0.5 ± 0.2
CXOU J013637.6 + 154717	4.6 ± 0.7	1.9 ± 0.5	1.9 ± 0.5	0.7 ± 0.3
CXOU J013637.7 + 154740	9.0 ± 1.0	2.7 ± 0.6	3.4 ± 0.6	2.9 ± 0.6
CXOU J013637.9 + 154749	2.1 ± 0.5	0.6 ± 0.2	1.0 ± 0.4	0.3 ± 0.2
CXOU J013638.8 + 154404	1.3 ± 0.4	1.1 ± 0.4	< 0.2	< 0.2
CXOU J013639.0 + 154755	5.7 ± 0.8	2.0 ± 0.5	2.1 ± 0.5	1.7 ± 0.4
CXOU J013639.1 + 154309	35.6 ± 2.1	11.0 ± 1.2	16.9 ± 1.4	7.4 ± 1.0
CXOU J013639.2 + 154600	3.0 ± 0.6	1.5 ± 0.4	1.0 ± 0.3	0.1 ± 0.1
CXOU J013639.3 + 154744	10.2 ± 1.1	< 0.1	2.3 ± 0.5	8.1 ± 0.9
CXOU J013639.4 + 154905	3.3 ± 0.6	2.0 ± 0.5	0.9 ± 0.3	0.3 ± 0.2
CXOU J013639.6 + 154830	2.4 ± 0.6	1.6 ± 0.4	0.5 ± 0.2	0.1 ± 0.1
CXOU J013639.6 + 154749	1.2 ± 0.4	1.0 ± 0.4	0.1 ± 0.1	< 0.1
CXOU J013640.0 + 154625	4.1 ± 0.7	2.5 ± 0.5	1.4 ± 0.4	< 0.1
CXOU J013640.3 + 154735	1.4 ± 0.4	1.2 ± 0.4	< 0.1	< 0.1
CXOU J013640.5 + 154928	6.9 ± 0.9	0.9 ± 0.3	3.1 ± 0.6	2.8 ± 0.6
CXOU J013640.6 + 154713	7.0 ± 0.9	2.5 ± 0.5	2.2 ± 0.5	2.2 ± 0.5
CXOU J013640.6 + 154647	4.0 ± 0.7	1.0 ± 0.4	1.7 ± 0.4	1.2 ± 0.4
CXOU J013641.0 + 154705	1.7 ± 0.5	0.4 ± 0.2	0.6 ± 0.2	0.4 ± 0.2
CXOU J013641.3 + 154650	1.0 ± 0.4	0.3 ± 0.1	0.4 ± 0.2	0.2 ± 0.1
CXOU J013641.6 + 155117	2.0 ± 0.5	< 0.1	0.1 ± 0.1	1.8 ± 0.5
CXOU J013641.6 + 154552	32.9 ± 1.9	7.9 ± 0.9	14.5 ± 1.3	10.5 ± 1.1

^a Foreground star

IAU Name	Count rate (0.3 – 8) keV	Count rate (0.3 – 1) keV	Count rate (1 – 2) keV	Count rate (2 – 8) keV
^b CXOU J013641.7 + 154701	18.7 ± 1.5	6.7 ± 0.9	7.3 ± 0.9	4.8 ± 0.7
CXOU J013641.9 + 154721	1.1 ± 0.4	1.2 ± 0.4	< 0.1	< 0.1
CXOU J013642.0 + 154430	1.3 ± 0.4	1.2 ± 0.4	0.1 ± 0.1	0.1 ± 0.1
CXOU J013642.0 + 154857	2.9 ± 0.6	0.6 ± 0.3	1.3 ± 0.4	0.8 ± 0.3
CXOU J013642.4 + 154701	2.2 ± 0.5	1.6 ± 0.4	0.3 ± 0.1	0.1 ± 0.1
CXOU J013643.2 + 154709	5.1 ± 0.8	0.6 ± 0.2	2.0 ± 0.5	2.3 ± 0.5
CXOU J013643.6 + 154742	4.5 ± 0.7	1.0 ± 0.3	1.8 ± 0.4	1.0 ± 0.4
CXOU J013643.8 + 154357	5.4 ± 0.8	1.0 ± 0.3	2.4 ± 0.5	1.8 ± 0.5
CXOU J013643.8 + 155022	4.1 ± 0.7	0.9 ± 0.3	1.8 ± 0.5	1.5 ± 0.4
CXOU J013644.0 + 154908	2.7 ± 0.6	0.4 ± 0.2	1.3 ± 0.4	0.9 ± 0.3
CXOU J013644.1 + 154818	31.1 ± 1.9	5.3 ± 0.8	16.5 ± 1.3	9.4 ± 1.0
CXOU J013644.3 + 154629	4.0 ± 0.7	3.2 ± 0.6	0.5 ± 0.2	0.3 ± 0.2
CXOU J013644.6 + 154848	1.4 ± 0.5	1.1 ± 0.4	0.1 ± 0.1	0.1 ± 0.1
CXOU J013644.9 + 154546	5.6 ± 0.9	1.7 ± 0.4	1.4 ± 0.4	2.0 ± 0.5
CXOU J013645.1 + 154837	1.4 ± 0.4	0.1 ± 0.1	0.5 ± 0.2	0.8 ± 0.2
CXOU J013645.2 + 154747	3.7 ± 0.7	1.5 ± 0.4	1.3 ± 0.4	0.2 ± 0.2
CXOU J013645.3 + 154910	2.7 ± 0.6	0.5 ± 0.2	1.1 ± 0.4	1.0 ± 0.4
CXOU J013646.0 + 154422	11.0 ± 1.2	1.9 ± 0.5	5.8 ± 0.8	3.1 ± 0.6
CXOU J013646.1 + 154842	3.1 ± 0.6	3.0 ± 0.6	0.1 ± 0.1	< 0.1
CXOU J013646.6 + 154611	0.7 ± 0.3	0.7 ± 0.3	< 0.1	< 0.1
^c CXOU J013647.4 + 154745	35.7 ± 2.0	28.5 ± 1.8	5.9 ± 0.8	0.8 ± 0.2
CXOU J013648.0 + 154445	1.8 ± 0.5	0.3 ± 0.2	1.3 ± 0.4	0.2 ± 0.1
CXOU J013648.8 + 154653	3.9 ± 0.7	0.7 ± 0.3	1.6 ± 0.4	1.5 ± 0.4
CXOU J013649.1 + 154527	5.2 ± 0.8	0.1 ± 0.1	0.9 ± 0.3	3.8 ± 0.7
CXOU J013650.0 + 154931	7.0 ± 0.9	1.2 ± 0.4	2.2 ± 0.5	2.8 ± 0.6
CXOU J013650.2 + 154915	9.6 ± 1.1	2.7 ± 0.6	3.9 ± 0.7	2.1 ± 0.5
CXOU J013650.3 + 155117	1.3 ± 0.4	< 0.1	0.6 ± 0.2	0.6 ± 0.2
CXOU J013651.1 + 154547	131.2 ± 3.9	60.5 ± 2.6	48.0 ± 2.3	23.3 ± 1.7
CXOU J013651.2 + 154339	13.5 ± 1.4	2.9 ± 0.6	8.1 ± 0.9	1.9 ± 0.5
CXOU J013651.8 + 155135	2.4 ± 0.6	0.6 ± 0.3	0.7 ± 0.3	0.8 ± 0.4
CXOU J013652.3 + 154737	9.4 ± 1.1	2.6 ± 0.6	4.3 ± 0.7	2.4 ± 0.6
CXOU J013653.0 + 155008	6.2 ± 0.9	1.3 ± 0.4	3.2 ± 0.6	1.1 ± 0.4
CXOU J013653.0 + 154510	1.7 ± 0.5	0.1 ± 0.1	0.6 ± 0.3	0.8 ± 0.3
CXOU J013653.8 + 154537	1.4 ± 0.5	< 0.1	0.1 ± 0.1	1.3 ± 0.4
CXOU J013654.4 + 154539	1.4 ± 0.5	0.4 ± 0.2	0.5 ± 0.3	0.3 ± 0.2
CXOU J013659.3 + 154631	5.6 ± 0.9	0.4 ± 0.2	1.4 ± 0.4	4.2 ± 0.7

^b Nucleus of M 74^c Foreground star